Phys Chem Minerals (1995) 22:200–206

PHYSICS AND CHEMISTRY OF MINERALS

© Springer-Verlag 1995

Static Compression and H Disorder in Brucite, $Mg(OH)_2$, to 11 GPa: a Powder Neutron Diffraction Study

M. Catti[1], **G. Ferraris**[2], **S. Hull**[3], **A. Pavese**[4]

[1] Dipartimento di Chimica Fisica ed Elettrochimica Università, via Golgi 19, I-20133 Milano, Italy
[2] Dipartimento di Scienze Mineralogiche e Petrologiche Università, via Valperga Caluso 37, I-10125 Torino, Italy
[3] ISIS Science Division, Rutherford Appleton Laboratory, Chilton Didcot, U.K.
[4] Dipartimento di Scienze della Terra (Sezione di Mineralogia), Università, via Botticelli 23, I-20133 Milano, Italy

Received July 27, 1994 / Revised, accepted January 28, 1995

Abstract. Neutron diffraction data suitable for Rietveld refinements were collected on a powder sample of synthetic $Mg(OH)_2$ by the Polaris time-of-flight spectrometer (ISIS spallation source, U.K.) at 10^{-4}, 7.8(3) and 10.9(6) GPa. The Paris-Edinburgh high-pressure cell with WC anvils was used. Pressure calibration and equation-of-state results were attained by separate runs with an NaCl internal standard. Interpolation of $p(V)$ data by the fourth-order Birch-Murnaghan e.o.s. yields $K_0=41(2)$ GPa, $K_0'=4(2)$ and $K_0''=1.1(9)$ GPa^{-1}. The bulk modulus obtained is smaller than previously reported results. Rietveld refinements ($R_{prof}=1.45\%$ and 2.02% at 10^{-4} and 10.9 GPa) show that H lies on the threefold axis (1/3, 2/3, z) up to 10.9 GPa, where a model with H disordered in (x, $2x$, z) can be refined. In the latter case, a hydrogen bond with $O-H=0.902(7)$, $H..O'=2.026(8)$ Å and $<OHO'=145.9(7)°$ is observed. Differences with previous results for deuterated brucite are discussed. The onset of H disorder, and a jump of the c/a ratio vs. pressure at 6–7 GPa, may be related to a second-order phase transition consistent with recently reported Raman spectroscopic results.

Introduction

Magnesium hydroxide, though present in limited amounts in the earth's crust, is considered to be of great importance as a potential source of water in the mantle, and also as a simple model material for the crystal-chemical behaviour of complex layered hydrous minerals. In particular, the phase relations and thermodynamic properties of brucite at high pressure have to be known to characterize the $Mg(OH)_2 \rightleftarrows MgO+H_2O$ equilibrium curve, which also constrains the thermodynamic behaviour of water in the upper mantle conditions (Johnson and Walker 1993). The thermal expansion of $Mg(OH)_2$ at room pressure has been determined (Redfern and Wood 1992). Shock wave experiments (Duffy et al. 1991) and recent measurements by X-ray synchrotron radiation have provided data for the equation of state of brucite to 78 GPa and 600 K (Fei and Mao 1993); however, more results are needed in the lower pressure range, in order to suitably constrain the bulk modulus value and the other elastic properties.

The crystal structure of $Mg(OH)_2$ is of CdI_2-type (Space group $P\bar{3}m1$; $Z=1$; Mg: 0, 0, 0; O and H: 1/3, 2/3, z), and is built up by (001) layers of $Mg(OH)_6$ coordination octahedra (Fig. 1). Neutron diffraction results at ambient conditions are reported by Zigan and Rothbauer (1967). The nature of interlayer bonding in brucite has been widely debated, and it seems due substantially to dispersion and polarization forces as in CdI_2 and $MgCl_2$, because the geometry of the OH environment appears to be quite unfavourable to hydrogen bonding (Bernal and Megaw 1935). However, other authors have argued in support of hydrogen bonding, on the basis of IR (Kruger et al. 1989) and Raman (Duffy et al. 1994) spectroscopic results showing a decrease of the O–H stretching frequency with increasing pressure. The latter study has also detected a sluggish pressure-dependent phase transition in brucite, supported by Raman data. Further, there has been recently a considerable theoretical interest in the subject, leading to two ab-initio quantum-mechanical Hartree-Fock studies (Sherman 1991; D'Arco et al. 1993). These simulate the structural behaviour at high pressure, concluding that the dispersive interlayer bonding does not change upon compression.

A structural study of brucite at high pressure by neutron diffraction has thus seemed to be desirable, in order to detect or rule out possible changes of the H atom surroundings consistent with hydrogen bonding. Results of a preliminary experiment to 2 GPa have been briefly reported (Catti et al. 1991). Other reasons concern the interest in deriving new data on the $p(V)$ equation of state, to get a more accurate elastic bulk modulus, and in exploring possible phase transitions of amorphization type, like that observed for $Ca(OH)_2$ (Meade and Jeanloz 1990).

Correspondence to: M. Catti

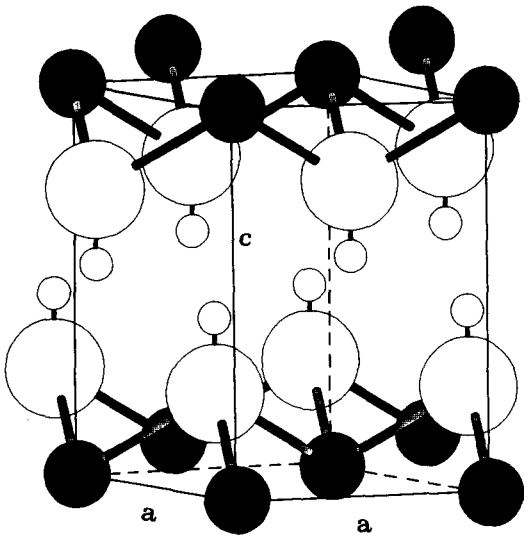

Fig. 1. Overview of the structure of $Mg(OH)_2$. *Full circles* represent Mg atoms; *large* and *small open circles* denote O and H atoms, respectively

When our experimental data had been already collected and analyzed, a similar investigation carried out on deuterated $Mg(OD)_2$ appeared (Parise et al. 1994). In the present case non-deuterated $Mg(OH)_2$ was used, despite the higher background radiation due to incoherent neutron scattering of hydrogen, because of our interest for the specific role of H rather than D atoms in hydrogen bonding geometry and related structural transformations. Thus a comparison of the two sets of results should be interesting, also considering that more emphasis was put on the equation-of-state in this study.

Experimental and Rietveld Refinements

A water solution of $MgCl_2$ was treated with KOH and boiled for a few hours, so as to improve the crystallinity of the precipitated powder. After intensive washing, the product was shown by X-ray diffraction to be pure $Mg(OH)_2$. Neutron diffraction data were collected on the Polaris time-of-flight powder diffractometer at the ISIS spallation source (Rutherford Appleton Laboratory, U.K.) in three experiments. The first one was carried out at room pressure on a 300 mm^3 sample in a vanadium can, using the C counter bank located at $2\Theta = 145°$; a single accurate powder pattern was obtained, to be used for Rietveld structure refinement.

The second experiment aimed at deriving a pressure calibration curve for $Mg(OH)_2$ in the Paris-Edinburgh cell (Besson et al. 1992), and also at studying the equation of state of that compound. A spherical pellet (86 mm^3) containing $Mg(OH)_2$ and NaCl in equal volumes was prepared and put between the WC anvils of the high-pressure cell. The pressure was increased in 11 steps, and each time a full diffraction pattern was collected for 2 hours on the B counter bank ($2\Theta = 90°$). Three Bragg peaks (2 0 2, 4 2 0 and 4 2 2) of NaCl and six (1 0 2, 1 0 3, 2 0 2, −2 0 3, 2 1 3, 3 1 2) of $Mg(OH)_2$ were used to determine the corresponding unit-cell edges (a and a, c, respectively), by means of least-squares refinements from d_{hkl} values. By linear interpolations between literature data of the NaCl equation of state $V(p)$ at room temperature (Decker 1971), the 11 pressure values were determined. These are reported in Table 1 together with the corresponding lattice constants of $Mg(OH)_2$ and with the estimated standard deviations. A full error propagation was applied to derive the e.s.d.'s of pressure, taking also into account the uncertainties reported for the NaCl equation of state (Decker 1971). The rocksalt cell edge used is 5.640 Å.

Table 1. Lattice constants of brucite $Mg(OH)_2$ measured vs. pressure by an NaCl internal standard. The e.s.d.'s are reported in parentheses

p (GPa)	a (Å)	c (Å)	c/a	V (Å^3)
0.48(3)	3.150(1)	4.720(2)	1.498(1)	40.56(4)
1.08(4)	3.141(3)	4.677(4)	1.489(3)	40.0(1)
2.8(1)	3.118(3)	4.591(3)	1.472(2)	38.7(1)
3.70(4)	3.108(6)	4.552(6)	1.465(5)	38.1(2)
4.4(1)	3.097(6)	4.529(7)	1.462(5)	37.6(2)
5.3(1)	3.087(8)	4.500(8)	1.458(6)	37.1(3)
6.3(3)	3.081(7)	4.471(9)	1.451(6)	36.8(2)
7.4(3)	3.085(5)	4.423(7)	1.434(5)	36.5(2)
8.2(3)	3.075(6)	4.402(7)	1.432(5)	36.0(2)
9.1(6)	3.063(6)	4.389(8)	1.433(5)	35.7(2)
9.9(5)	3.055(3)	4.375(4)	1.432(3)	35.4(1)

In the third experiment, a spherical pellet of pure $Mg(OH)_2$ was used in the Paris-Edinburgh cell. The pressure was brought at first to 7.8 GPa, and then to 10.9 GPa, recording full powder patterns on the B counter bank (18 and 24 hours, respectively) suitable for Rietveld refinements. The real pressure values were determined by interpolating the measured lattice constants of $Mg(OH)_2$ in the calibration results of the previous experiment, as described below. Direct use of NaCl as internal standard would have reduced the sample volume and the intensity statistics too much.

In all runs carried out at high pressures the collected intensity profiles were corrected for absorption due to the WC anvils.

Rietveld profile refinements were carried out on the three sets of data collected in the first and third experiments, employing the GSAS programme (Larson and Von Dreele 1986). The peak shape was treated by two exponential functions (instrumental and moderator contribution) convoluted with a linear combination of Gaussian (σ half-width) and Lorentzian (γ half-width) components (pseudo-Voigt function, sample contribution). The dependences of the σ and γ parameters on d_{hkl} are expressed as follows: $\sigma^2 = \sigma_0^2 + \sigma_1^2 d_{hkl}^2 + \sigma_2^2 d_{hkl}^4$ and $\gamma = \gamma_1 d_{hkl} + \gamma_2 d_{hkl}^2$. The background was described by Chebyschev polynomials. Preferential orientation was corrected for properly (Larson and Von Dreele 1986): the [001] direction is preferentially normal or parallel to the incident beam in the room- or high-pressure experiment, respectively.

Both the ordered structural model of Zigan and Rothbauer (1967), with H on the threefold axis (1/3, 2/3, z),

Table 2. Numbers of (total and structural) variables and of observations, unweighted and weighted R profile indexes and χ^2 for the four Rietveld refinements at three different pressures. The last column refers to the H atom off the threefold axis with isotropic thermal factor

	p (GPa)			
	10^{-4}	7.8	10.9	
total var.	23	22	22	22
struct. var.	8	8	8	8
n. obs.	3572	3160	3156	3156
R (prof.)	1.45	2.46	2.01	2.02%
R_w (prof.)	1.13	1.77	1.66	1.65%
χ^2	2.09	1.43	1.43	1.41%

Table 3. Rietveld refined structural parameters [lattice constants (Å), atomic fractional coordinates and displacement factors (Å^2)] of brucite $Mg(OH)_2$ at room and high pressures. The e.s.d.'s are reported in parentheses

	p (GPa)			
	10^{-4}	7.8	10.9	
a	3.14979(4)	3.0698(7)	3.0467(5)	3.0464(5)
c	4.7702(1)	4.429(1)	4.3554(9)	4.3553(8)
z(O)	0.2203(3)	0.2357(9)	0.2470(8)	0.2473(8)
x(H)	1/3	1/3	1/3	0.3371(15)
z(H)	0.4130(6)	0.4415(21)	0.4480(15)	0.4474(14)
B(Mg)	0.43(2)	1.0(1)	0.05(6)	0.01(6)
B(O)	0.42(1)	0.61(9)	0.18(6)	0.18(6)
B(H)				0.7(2)
B_{11}(H)	3.31(4)	2.8(2)	3.0(2)	
B_{33}(H)	0.82(8)	3.5(4)	1.1(2)	

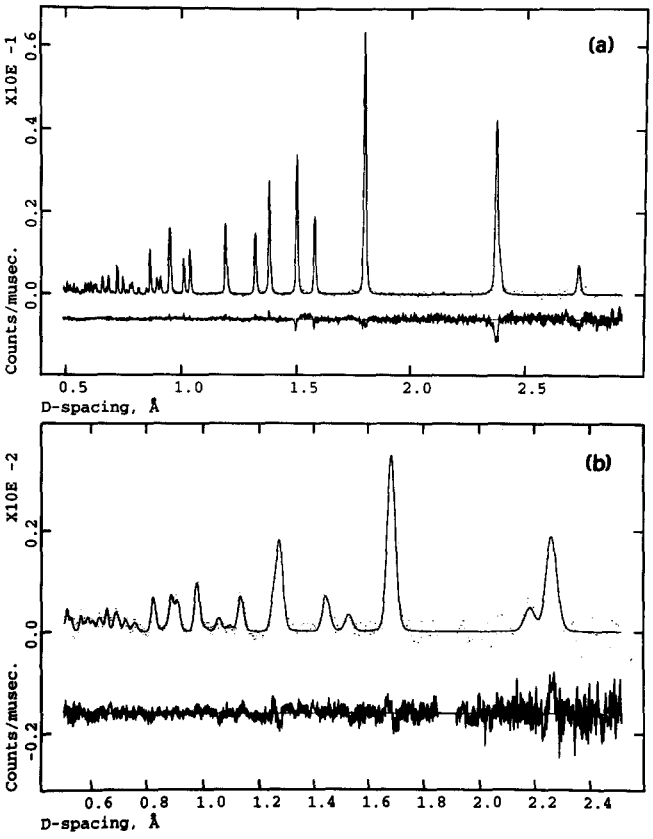

Fig. 2. Experimental (*dots*) and computed (Rietveld refinement, *full line*) diffraction profiles of $Mg(OH)_2$ at room pressure (**a**) and at 10.9(6) GPa (**b**)

and that proposed by Parise et al. (1994) with H disordered over three equivalent positions (x, $2x$, z) were tried. Only the ordered model converged with data collected at ambient pressure and 7.8 GPa. On the other hand, convergence was attained with both models and very similar agreement R factors using data at the highest pressure. Thus results are reported in Tables 2 (statistical indexes) and 3 (final structural parameters) for four refinements. The Mg and O thermal ellipsoids turned out to be isotropic within the e.s.d.'s, so that in the final cycles they were constrained to isotropy. Experimental, computed and difference diffraction profiles are shown in Fig. 2 for results at room pressure and at 10.9 GPa. The profile at high pressure is already corrected for absorption. The much smaller signal-to noise ratio of the high- with respect to room-pressure data should be remarked. Besides, the peak widths are increased considerably: the σ_1^2 coefficient increases by nearly 20 times from 10^{-4} to 11 GPa. It should be noticed that the displacement factors obtained at high pressure are not fully satisfactory (cf. the B_{33}(H) value at 7.8 GPa, and the very small value of B(Mg) at 10.9 GPa). This may be partly due to the features remarked above, and partly to insufficient correction of the absorption effects due to the high-pressure cell. The absorption problem can affect the accuracy of diffraction results at high pressure severely, and thermal parameters are of course most sensitive to systematic errors. The incoherent scattering of H atoms, though contributing significantly to the background, did not cause problems in the Rietveld refinements.

Equation of State and Elastic Properties

The a and c unit-cell edges are plotted versus pressure in Fig. 3, including the room pressure values coming from Rietveld refinement (Table 3). Regular trends appear in the two curves up to 6 GPa, while slight positive (a) and negative (c) jumps are observed aroud 7 GPa. The discontinuity is more evident by plotting the c/a ratio against p (Fig. 4): after decreasing regularly, a sharp drop is observed at about 7 GPa, while at larger pressures the trend is constant. This effect might be due to non-hydrostaticity of the applied pressure, but is nonetheless observed also in X-ray data reported by Fei and Mao (1993). Thus the c/a discontinuity may correspond to some sort of second-order structural change, consistently with the spectroscopic results which suggest a sluggish phase transition beginning above 4 GPa (Duffy et al. 1994). However, further experimental work is needed to exclude non-hydrostatic stress effects.

Linear (a) and parabolic (c, c/a) least-squares approximations were carried out for the pressure dependencies

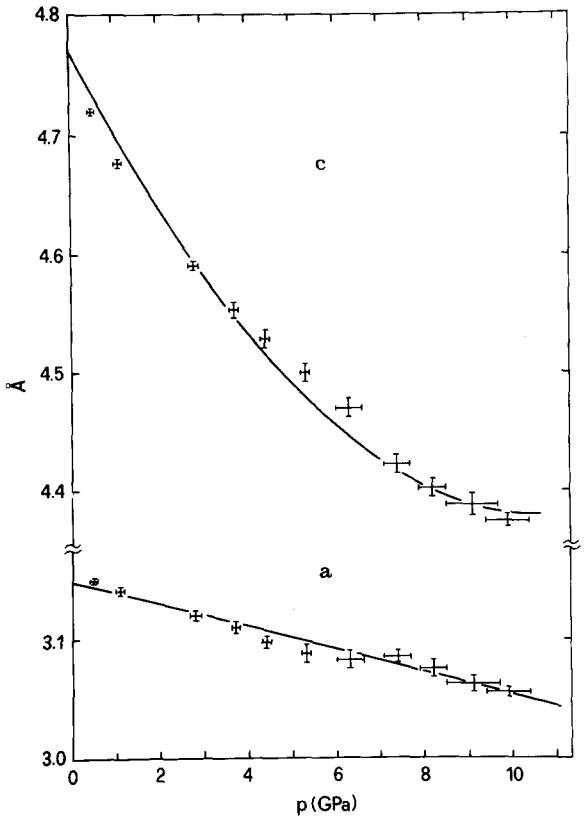

Fig. 3. Unit-cell edges of brucite $Mg(OH)_2$ vs. pressure. Least-squares interpolating curves are shown

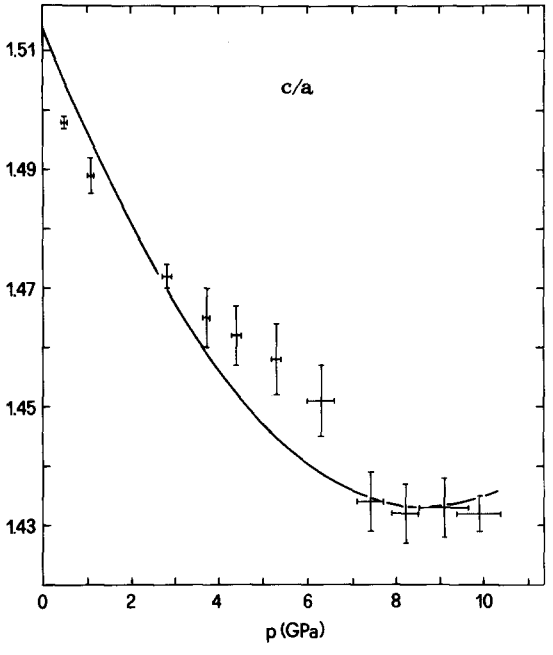

Fig. 4. Ratio of the c to a cell edge vs. pressure. A least-squares interpolation parabola is shown

of lattice parameters (12 points including room-pressure values from Table 3), using weights related to the e.s.d.'s of the cell edges. The following results were obtained (room-mean-square deviations of 0.006 and 0.01 Å, and of 0.007, respectively):

$$a = 3.150 - 0.0096p,$$
$$c = 4.770 - 0.0732p + 0.0034p^2,$$
$$c/a = 1.514 - 0.0189p + 0.0011p^2.$$

Weak but significant deviations of the experimental points from the corresponding curves are observed for $a(p)$ and $c(p)$ in Fig. 3, because of the small jumps discussed above. The deviations are much larger for c/a (Fig. 4). Polynomials of order higher than two were not tried to avoid unphysical inflexion points. Interpolations in the lower pressure range ($p < 5$ GPa) were also performed for a and c, obtaining the following results:

$$a = 3.150 - 0.0101p,$$
$$c = 4.764 - 0.0828p + 0.0068p^2 \quad (p < 5\,\text{GPa}).$$

These are particularly useful for deriving the zero-pressure slopes of the $a(p)$ and $c(p)$ curves, corresponding to the coefficients of the first-order terms in the pressure expansions. The linear compressibilities of the unit-cell edges are given by (Catti 1992; Catti et al. 1994):

$$(a/a_0 - 1)/p = -(s_{11} + s_{12} + s_{13}),$$
$$(c/c_0 - 1)/p = -(s_{33} + 2s_{13});$$

where s_{ij} $(i, j = 1, \ldots, 6)$ are the elastic compliance coefficients. The linear incompressibilities (at zero pressure) K_{0a} and K_{0c} are the reciprocal of the above expressions. By truncation to first-order of the lower pressure expansions, one obtains the following values:

$$s_{11} + s_{12} + s_{13} = 0.0032\ \text{GPa}^{-1}, \quad K_{0a} = 313\ \text{GPa};$$
$$s_{33} + 2s_{13} = 0.0174\ \text{GPa}^{-1}, \quad K_{0c} = 57\ \text{GPa}.$$

The volume compressibility $s_{33} + 2s_{11} + 2s_{12} + 4s_{13}$ amounts to 0.0238 GPa^{-1}, whence a bulk elastic modulus of 42 GPa is obtained.

The unit-cell volume is plotted against pressure in Fig. 5. A finite strain analysis can be usefully applied to interpret these data. The Birch-Murnaghan equation of state truncated to third-order in the Eulerian finite strain parameter (Birch 1978) has the following form:

$$p = \frac{3}{2} K_0 \left(\frac{V_0}{V}\right)^{5/3} \left[\left(\frac{V_0}{V}\right)^{2/3} - 1\right] \cdot \left\{1 + \frac{3}{4}(K_0' - 4)\left[\left(\frac{V_0}{V}\right)^{2/3} - 1\right]\right\},$$

where K_0 and K_0' are the bulk elastic modulus and its pressure derivative, respectively, at room (zero) pressure, and V_0 is 40.986(2) Å^3 (room-pressure cell of Table 3). The fourth-order approximation formula includes the following quadratic term to be inserted into the graph brackets of the above expression:

$$\frac{3}{8} K_0 K_0'' + (K_0' - 4)(K_0' - 3) + \frac{35}{9}\left[\left(\frac{V_0}{V}\right)^{2/3} - 1\right]^2;$$

K_0'' is the second pressure derivative of the bulk modulus at zero pressure. The $p(V)$ experimental points obtained

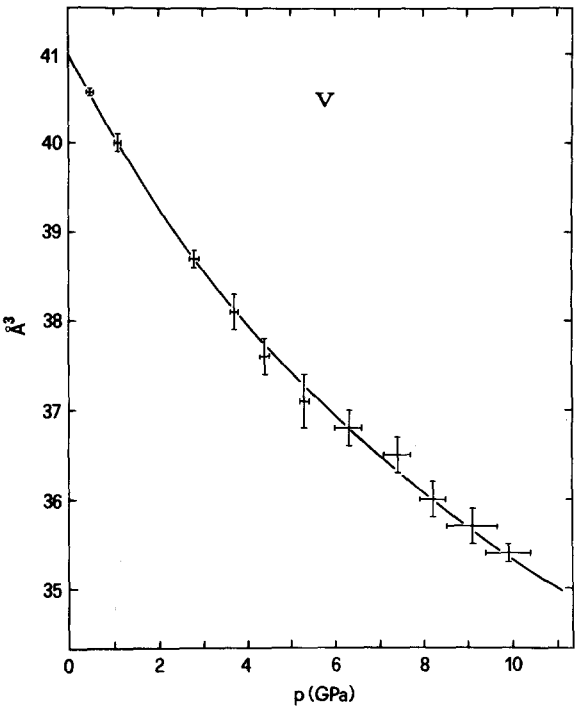

Fig. 5. Unit-cell volume of brucite $Mg(OH)_2$ vs. pressure. The interpolating third-order Birch-Murnaghan equation of state is shown

for $Mg(OH)_2$ were least-squares fitted to these interpolation formulae by means of the BIRCH 2.0 computer programme (Ross and Webb 1990). The third-order approximation gave 39(1) GPa and 7.6(7) for the two unknown parameters K_0 and K'_0, respectively. The bulk modulus obtained in this way is slightly smaller than that coming from polynomial approximations of the cell edges in the lower pressure range. By using the fourth-order expression the values $K_0 = 41(2)$ GPa, $K'_0 = 4(2)$ and $K''_0 = 1.1(9)$ GPa^{-1} are calculated. The agreement with the K_0 value from linear compressibilities of the cell edges is now very good.

Use of the $p(V)$ equation of state of brucite allowed us to interpolate the volume values derived from the two high-pressure Rietveld refinements [36.15(2) and 35.00(2) Å^3, respectively, cf. lattice constants of Table 3], so as to determine the corresponding pressures of 7.8(4) and 10.9(6) GPa.

A substantial discrepancy is observed between the bulk modulus and its pressure derivative obtained here for brucite, and previous results from a synchrotron X-ray diffraction static compression experiment (Fei and Mao 1993). The values of $K_0 = 54(2)$ GPa and $K'_0 = 4.7(2)$ reported in the latter study would indicate a stiffer $Mg(OH)_2$ structure, consistently also with shock wave measurements (Duffy et al. 1991). However, unit-cell data were collected by Fei and Mao (1993) in the range 2.6–33.1 GPa. By using only their volume values below 10 GPa, a fit to the third-order Birch-Murnaghan e.o.s. gives $K_0 = 48(4)$ GPa and $K'_0 = 7(2)$, while the fourth-order fit does not converge. It is important to stress that K_0 is defined as a zero pressure slope, and thus data in the low pressure range are very important to constrain it correctly. This suggests that shock wave results, usually obtained for $p > 10$ GPa, should be considered with particular caution. We would conclude that the value of 48(4) GPa is probably still overestimated, because of the lack of data for $p < 2$ GPa. The bulk modulus of brucite is thus likely to lie closer to 40 than to 50 GPa; measurements of elastic constants by ultrasonic methods or Brillouin scattering are needed to obtain a more accurate value. An X-ray static compression experiment on $Ca(OH)_2$, portlandite, gave $K_0 = 38(2)$ GPa and $K'_0 = 5.2(7)$ (Meade and Jeanloz 1990). By comparison with $Ca(OH)_2$, magnesium hydroxide turns out to be slightly stiffer. However, the difference is mainly due to the a edge incompressibility (313 vs. 192 GPa), related to the Mg–O bond being more rigid than Ca–O. On the other hand, the two K_{0c} values (57 and 60 GPa) are similar, indicating that the interlayer compressibility is independent of the nature of the cation Mg or Ca.

Crystal Structure at Variable Pressure

The relevant interatomic distances and angles of brucite at different pressures are reported in Table 4. Because of the much larger thermal displacement of H with respect to O normal to the O–H direction, that bond length is underestimated and can be corrected by the approximate formula (Busing and Levy 1957):

$$d(\mathrm{O-H}) = [c^2(z(\mathrm{H}) - z(\mathrm{O}))^2 + 2(B_{11}(\mathrm{H}) - B_{11}(\mathrm{O}))/8\pi^2]^{1/2}.$$

The values obtained are reported in Table 4 as well.

The structural results at ambient conditions confirm closely those obtained previously on natural brucite (Catti et al. 1991). They should also be compared with older neutron diffraction data (Zigan and Rothbauer 1967), which were based on the intensities of 46 single-crystal reflexions belonging to the *h0l* and *hhl* classes. A significant difference is observed for the z(H) coordinate [0.4303(12)] and the related O–H distance [0.995(8) Å uncorrected, 1.029 Å corrected], which are larger than the present results. If we consider the O–H bond length of 0.98(2) Å determined in brucite by solid state N.M.R. (Elleman and Williams 1956), and the spectroscopic values of 0.958 and 0.971 Å reported by Busing and Levy (1957) for gas-phase H_2O and OH^-, respectively, our result of 0.958 Å (corrected for thermal motion) appears to be more reliable than that of the older study. As for the geometry of the H atom environment, the results of Zigan and Rothbauer (1967) are substantially confirmed. H is equidistant from three O′ atoms related by the threefold axis, and belonging to the oxygen layer adjacent to that of O. The large H…O′ distances and the very bent <OHO′ angles would be unfavourable for a normal hydrogen bond, but a possible trifurcated hydrogen bond, consistent with larger distortions, cannot be ruled out. For six cases of bifurcated H bridges of H_2O molecules examined by Chiari and Ferraris (1982), average values of H…O′ = 2.353 Å, O…O′

Table 4. Interatomic distances (Å) and <OHO′ angle (°) in brucite $Mg(OH)_2$ at room and high pressures. The e.s.d.'s are given in parentheses. For the O−H bond length, values corrected for thermal motion are reported on the second line

	p (GPa)			
	10^{-4}	7.8	10.9	
Mg−O	2.1003(6)×6	2.057(2)×6	2.062(2)×6	2.062(2)×6
O−H	0.919(3)	0.912(9)	0.875(8)	0.902(7)
O−H (corr.)	0.958(3)	0.942(12)	0.915(11)	0.909(10)
H...O′	2.523(2)×3	2.277(7)×3	2.204(4)×3	2.026(8) 2.307(5)×2
O...O′	3.229(2)×3	2.937(6)×3	2.820(6)×3	2.818(5)×3
H...H′	1.999(2)×3	1.846(5)×3	1.816(3)×3	2.042(8) 1.718(5)×2
<OHO′	133.89(5)×3	128.9(2)×3	127.1(2)×3	145.9(7) 115.7(4)×2

=3.075 Å and <OHO′=134.6° are observed, instead of the corresponding values of 1.979 Å, 2.878 Å and 157.2° for normal H bonds.

By considering the effect of pressure on the crystal structure, the most striking result is that only at the highest compression (10.9 GPa) a model with the H atom disordered off the threefold axis can be refined successfully, and yet with equal agreement factor as the traditional model. This contrasts with results obtained on deuterated brucite by Parise et al. (1994), who refined the disordered model on data collected at 0.4, 1.9, 5.4 and 9.3 GPa. Thus disordering under pressure seems to occur much more easily for deuterium than for hydrogen in the brucite structure.

In the disordered structure the strong anisotropy of thermal motion of hydrogen disappears. Locally, H approaches one of the three neighbouring O′ atoms, and geometrical conditions much more favourable for hydrogen bonding are set up: the H...O′ distance diminishes and the <OHO′ angle widens substantially (Table 4). Further, the H...H′ spacing increases releasing the repulsive interatomic stress due to compression. Thus at some pressure the disordered structure has to become energetically favoured, because attractive and repulsive interactions increase and decrease, respectively. The O−H bond length hardly shortens from 10^{-4} to 10.9 GPa, if the disordered structure is assumed at high pressure, while it would decrease substantially by keeping the ordered structure model. This is again different from results for the deuterated sample (Parise et al. 1994), where the O−D distance increases from 0.95(1) to 1.021(9) Å at 0.4 and 9.3 GPa, respectively. Such a behaviour would indicate that hydrogen bonding in brucite strengthens with pressure more for D than for H atoms, consistently with what stressed above for their disordering effect. However, it is interesting to compare these results with those obtained in a similar neutron diffraction high-pressure study on deuterated ice VIII (Nelmes et al. 1993). In that case, where hydrogen bonding is surely present, the O−D bond length is found to remain constant to 10 GPa, while O...O′ and D...O′ shorten substantially.

Let us now consider the relations of our structural results with IR (Kruger et al. 1989) and Raman (Duffy et al. 1994) spectroscopic data at high pressure on brucite. These show a decrease of frequency of the OH stretching modes with pressure ($\partial \ln \nu/\partial p = -1.6\times10^{-4}$ and -2.0×10^{-3} GPa^{-1} for IR and Raman frequencies, respectively), but smaller than that observed for ice VIII (-7.3×10^{-3} GPa^{-1}, IR data after Klug and Whalley 1984). As interpretation, it has been often surmised that hydrogen bonding arises or becomes stronger with increasing pressure. This is based on calculations employing potential functions independent of p, which lead to a prediction of increasing O−H length as O...O′ decreases at high pressure (Klug and Whalley 1984). However, the structural evidence gathered so far is not fully consistent with this model, since O−H remains nearly constant with compression in ice VIII and in $Mg(OH)_2$. As argued by Nelmes et al. (1993), it may not be correct to treat the O−H potential as pressure indpendent, and there is no reason to assume that O−H and O...O′ under pressure are related similarly as in the average O−H...O′ bond under varying chemical environments at room pressure. On the other hand, the spectroscopic argument seems to definitely support the disordered rather than ordered structural model at 10.9 GPa, because in the latter case a significant contraction of the O−H length would be observed.

Conclusions

Some structural indications have been obtained, supporting the sluggish pressure-driven phase transformation of $Mg(OH)_2$ observed from Raman spectroscopic data. A disordered structural model with H off the threefold axis has been refined at 10.9 GPa; that structure probably corresponds to local ordered domains lacking the symmetry axis (static disorder). Thus a definite tendency to transform a very weak, if any, trifurcated H bond into a true hydrogen bonding is observed in brucite at high pressure, improving the inter-layer cohesion and decreasing the H...H′ repulsion. The displacement of H from the threefold axis is expected to increase continuously for pressures exceeding that attained, so as to strengthen the H bonding even more. This process seems however to occur at higher pressure than in deuterated brucite. Further, it could account possibly for the new peak reported in the Raman spectrum of brucite at $p>4$ GPa and absent at lower pressures (Duffy et al. 1994). Finally, the measured lattice constants indicate,

in the lower p range, a substantially softer structure for brucite with respect to previous published X-ray data.

Acknowledgements. We thank J.S. Loveday and R.J. Nelmes for very useful suggestions and discussions, and T.S. Duffy for sending us a preprint of his Raman study of brucite. Financial support from C.N.R. anglo-italian project (Roma), M.U.R.S.T. (Roma), C.S.I. Piemonte and CS Geodinamica delle Catene Collisionali (C.N.R. Torino) is gratefully acknowledged.

References

Bernal JD, Megaw HD (1935) The function of hydrogen in intermolecular forces. Proc Roy Soc London 151A:384–420

Besson JM, Nelmes RJ, Hamel G, Loveday JS, Weill G, Hull S (1992) Neutron powder diffraction above 10 GPa. Physica B 180–181:907–910

Birch F (1978) Finite strain isotherm and velocities for single-crystal and polycrystalline NaCl at high pressures and 300 K. J Geophys Res 83:1257–1267

Busing WR, Levy HA (1957) Neutron diffraction study of calcium hydroxide. J Chem Phys 26:563–568

Catti M (1992) Physical properties of crystals. In: Giacovazzo C (ed) Fundamentals of crystallography, Chapter 9. Oxford University Press, Oxford

Catti M, Ferraris G, Hull S (1991) Powder neutron diffraction study of brucite and gibbsite and pressure dependence of the structure of $Mg(OD)_2$. XIII European Crystallographic Meeting, Ljubliana-Trieste, 26–30 August 1991, Book of abstracts: 316

Catti M, Ferraris G, Hull S, Pavese A (1994) Powder neutron diffraction study of $2M_1$ muscovite at room pressure and at 2 GPa. Eur J Mineral 6:171–178

Chiari G, Ferraris G (1982) The water molecule in crystalline hydrates studied by neutron diffraction. Acta Crystallogr B38:2331–2341

D'Arco Ph, Causà M, Roetti C, Silvi B (1993) Periodic Hartree-Fock study of a weakly bonded layer structure: brucite $Mg(OH)_2$. Phys Rev B47:3522–3529

Decker DL (1971) High-pressure equation of state for NaCl, KCl, and CsCl. J Appl Phys 42:3239–3244

Duffy TS, Ahrens TJ, Lange MA (1991) The shock wave equation of state of brucite $Mg(OH)_2$. J Geophys Res 96:14319–14330

Duffy TS, Meade C, Fei Y, Mao HK, Hemley RJ (1994) High-pressure phase transition in brucite $Mg(OH)_2$. Submitted to Am Mineral

Elleman DD, Williams D (1956) Proton positions in brucite crystals. J Chem Phys 25:742–744

Fei Y, Mao HK (1993) Static compression of $Mg(OH)_2$ to 78 GPa at high temperature and constraints on the equation of state of fluid H_2O. J Geophys Res 98:11875–11884

Johnson MC, Walker D (1993) Brucite [$Mg(OH)_2$] dehydration and the molar volume of H_2O to 15 GPa. Am Mineral 78:271–284

Klug DD, Whalley E (1984) The uncoupled O–H stretch in ice VII. The infrared frequency and integrated intensity up to 189 kbar. J Chem Phys 81:1220–1228

Kruger M, Williams Q, Jeanloz R (1989) Vibrational spectra of $Mg(OH)_2$ and $Ca(OH)_2$ under pressure. J Chem Phys 91:5910–5915

Larson AC, Von Dreele RB (1986) GSAS: General structure analysis system manual. Los Alamos National Laboratory Report LAUR 86–748

Meade C, Jeanloz R (1990) Static compression of $Ca(OH)_2$ at room temperature: observations of amorphization and equation of state measurements to 10.7 GPa. Geophys Res Lett 17:1157–1160

Nelmes RJ, Loveday JS, Wilson RM, Besson JM, Pruzan Ph, Klotz S, Hamel G, Hull S (1993) Neutron diffraction study of the structure of deuterated ice VIII to 10 GPa. Phys Rev Lett 71:1192–1195

Parise JB, Leinenweber K, Weidner DJ, Tan K, Von Dreele RB (1994) Pressure-induced H bonding: neutron diffraction study of brucite, $Mg(OD)_2$, to 9.3 GPa. Am Mineral 79:193–196

Redfern SAT, Wood BJ (1992) Thermal expansion of brucite, $Mg(OH)_2$. Am Mineral 77:1129–1132

Ross CR II, Webb SL (1990) BIRCH, a program for fitting PV data to an Eulerian finite-strain equation of state. J Appl Cryst 23:439–440

Sherman DM (1991) Hartree-Fock band structure, equation of state, and pressure-induced hydrogen bonding in brucite, $Mg(OH)_2$. Am Mineral 76:1769–1772

Zigan F, Rothbauer R (1967) Neutronenbeugungsmessungen am Brucit. N Jahrb Mineral Monatsh:137–143